Designing a highly bioactive 3D bone-regenerative scaffold by surface immobilization of nano-hydroxyapatite

Sung Eun Kim,[a] Hyung Woo Choi,[a] Hong Jae Lee,[a] Jeong Ho Chang,[a] Jinsub Choi,[a] Kyung Ja Kim,[a] Hee Jin Lim,[b] Young Joon Jun[c] and Sang Cheon Lee*[a]

Received 18th June 2008, Accepted 1st August 2008
First published as an Advance Article on the web 18th September 2008
DOI: 10.1039/b810328c

A novel approach to the fabrication of porous scaffolds with surface-immobilized nano-hydroxyapatite (N-HAp) is developed for effective bone tissue engineering. The discrete nano-level anchoring of N-HAp on the pore surface of chitosan scaffolds is achieved using surface-repellent stable colloidal N-HAp with surface phosphate functionality. Field-emission scanning electron microscopy (FE-SEM) and X-ray photoelectron spectroscopy (XPS) confirm pronounced exposure of N-HAp on the surfaces of chitosan scaffolds at the nano-level, which can not be accomplished with the conventional polymer/N-HAp composite scaffolds. This rational surface engineering enables surface-anchored N-HAp to express its overall intrinsic bioactivity, since N-HAp is not phase-mixed with the polymers. The porous chitosan scaffolds with surface-immobilized N-HAp provide more favorable environments than conventional bulk phase-mixed chitosan/N-HAp scaffolds in terms of cellular interaction and growth. *In vitro* biological evaluation using alkaline phosphatase activity assay supports that immobilized N-HAp on pore surfaces of chitosan scaffolds contributed to the more enhanced *in vitro* osteogenic potential. In addition, scaffolds with surface-exposed N-HAp provide favorable environments for enhanced *in vivo* bone tissue growth, estimated by characteristic biomarkers of bone formation such as collagen. The results suggest that the newly developed hybrid scaffolds with surface-immobilized N-HAp may serve as useful 3D substrates with pore surfaces featuring excellent bone tissue-regenerative properties.

Introduction

The combination of biopolymers and nanophase calcium phosphate, particularly nano-hydroxyapatite (N-HAp), is recognized as an attractive approach for generating hybrid scaffolds for bone regeneration because it can provide a favorable environment for bone-tissue growth.[1–4] Its usefulness is easily understood by considering the structure of natural bones in which the main components are inorganic N-HAp and organic collagen-based fibrils.[5,6] In the field of tissue engineering, three-dimensional porous polymer scaffolds not only play a primary role in the manipulation of cell functions but also guide new tissue growth at defective sites.[7–9] Therefore, there has been growing interest in fabricating hybrid three-dimensional porous scaffolds displaying the synergistic benefits of biocompatible polymers and N-HAp.[1,2,10]

To develop high-performance bone-regenerative materials, surface engineering of scaffold pores is one of the most important considerations since this determines whether the cells can effectively adhere, migrate, and proliferate on the porous scaffolds.[11] Thus, nanoscale engineering of scaffold pore surfaces with the highly bioactive N-HAp can be recognized as an ideal approach for useful production of hybrid scaffolds for bone-tissue regeneration. To date, most fabrication methods for three-dimensional hybrid scaffolds are based on simple physical mixing of a polymer and N-HAp in a solution or bulk state. Examples are hybrid scaffolds fabricated by liquid–liquid or solid–liquid phase separation, solvent casting/particulate leaching, and gas forming/particulate leaching.[1,2,10] However, these approaches are not effective for stably placing N-HAp on the pore surface of polymer scaffolds at the nano-level. Furthermore, N-HAp tends to form large micro-scale aggregates and to mix with polymer bulk phases with a low interfacial affinity. Although template-driven biomineralization is utilized as a promising alternative approach to hybrid scaffolds, the homogeneous/uniform growth of N-HAp, in terms of crystal size and nucleation location, is limited due to non-controlled growth behavior on surfaces.[12–14] Furthermore, it usually requires a time-consuming incubation process in a simulated body fluid.[15,16] Therefore, current approaches have limitations in expressing the intrinsic bioactive physicochemical properties of N-HAp originating from large specific surface areas, such as osteoconductivity and high affinity with serum proteins, which facilitate cellular adhesion.[17,18] Hence, for hybrid scaffolds to express the overall benefits of N-HAp itself, it is desirable to develop a novel fabrication method that can expose N-HAp without aggregation on the pore surface of polymer scaffolds.

Herein, we report on an unprecedented synthetic approach to porous hybrid scaffolds with immobilized N-HAp on the pore

[a]*Nanomaterials Application Division, Korea Institute of Ceramic Engineering and Technology, 233-5 Gasan-Dong, Guemcheon-Gu, Seoul, 153-801, Korea. E-mail: sclee@kicet.re.kr; Fax: +82-2-3282-7811; Tel: +82-2-3282-2469*
[b]*Department of Neurobiology, College of Medicine, The Catholic University of Korea, Seoul, 137-701, Korea*
[c]*Department of Plastic Surgery, College of Medicine, The Catholic University of Korea, Seoul, 137-701, Korea*

surface of chitosan scaffolds. 'Surface' and 'interface' are two key words that characterize our approach. In order to provide the 'surface' with a highly cell-compatible environment by incorporating inorganic N-HAp on polymers, the first subject to address is how to overcome the intrinsic low affinity at the 'interface' between inorganic N-HAp and organic chitosan. To meet this concern, the main technology employed in this strategy is to use rationally surface-modified N-HAp with organic polymer species. Because the stable nano-level dispersion of N-HAp in solutions is critical in anchoring N-HAp homogeneously and uniformly on the pore surfaces, chemical or physical treatments of N-HAp surfaces that can afford the surface reactivity and extremely high colloidal stability are prerequisite. Recently, we have reported preliminary results on the novel synthesis procedure for chemical grafting of anionic poly(ethylene glycol methacrylate phosphate) (PolyEGMP) on the surface of N-HAp.[19] Since the phosphate anionic groups of PolyEGMP can provide N-HAp with surface reactivity and aqueous colloidal stability, the use of PolyEGMP-grafted N-HAp can be recognized as a good choice to immobilize N-HAp on pore surfaces of chitosan scaffolds. We are interested in knowing whether the presence of surface-immobilized N-HAp can provide more favorable scaffold surfaces than conventional bulk phase-mixed N-HAp in terms of cellular interaction, osteogenesis, and bone tissue growth. Surface immobilization of N-HAp on scaffold pore surfaces was performed by the reaction of PolyEGMP-grafted N-HAp with primary amine groups on chitosan surfaces. Morphological and elemental analyses of surfaces of hybrid scaffolds were carried using field-emission scanning electron microscopy (FE-SEM) and X-ray photoelectron spectroscopy (XPS). The significant effect of surface-immobilized N–HAP on *in vitro* and *in vivo* osteogenic potential and bone regeneration was discussed.

Experimental

1. Preparation of polyEGMP-grafted N-HAp

The grafting polymerization of EGMP on the surface of N-HAp was performed by a procedure established in our laboratory.[19] In brief, surface-reactive thiol-functionalized N-HAp (N-HAp-SH) was firstly synthesized by an *in situ* synthesis procedure. A mixed aqueous solution (200 mL) of H_3PO_4 (0.3 M) and 3-mercaptopropionic acid (0.06 M) was added dropwise to vigorously stirred distilled water (200 mL) solution of $Ca(OH)_2$ (0.25 M), at a rate of 1 mL min^{-1} at 60 °C. At pH 7.0, N-HAp-SH was purified by several washes with double distilled water and freeze-dried. The number of surface thiol groups per g N-HAp, by Ellman's reagent analysis, was calculated to be 3100 ± 250, which corresponds to 1.8×10^{-6} mol thiol groups per g HAp. In brief, N-HAp-SH (2.5 g) in 50 mL of *N*,*N*-dimethylformamide (DMF) was treated in a bath-type ultrasonicator for 30 min, and the uniformly dispersed solution was degassed by N_2 bubbling for 30 min. To this suspension, EGMP and 2,2′-azobisisobutyronitrile (0.02 g) in DMF (1 mL) were added at 60 °C, and the reaction was maintained under N_2 for 20 h. After the reaction, PolyEGMP-grafted N-HAp was purified and collected by repeated washing with an aqueous solution of sodium hydroxide (1 M) and centrifugation at 3000 rpm for 20 min (×5). The final product was obtained by freeze-drying.

2. Estimation of kinetic colloidal stability of N-HAp and PolyEGMP-grafted N-HAp

Stability kinetics of N-HAp and PolyEGMP-grafted N-HAp colloids in aqueous phase were estimated by time-dependent changes of back scattering intensities. The analyzed dispersion was contained in a cylindrical glass measurement cell. The light source was a pulsed near infrared light source (880 nm), which was positioned at 5 mm height from the bottom of 40 mm high sample solutions. A synchronous optical sensor receive light back scattered by the sample (135° from the incident radiation, backscattering detector) using Turbiscan LAb^{Expert} (Formulaction, France).

3. Surface immobilization of N-HAp on pore surfaces of chitosan scaffolds

Immobilization of N-HAp on chitosan scaffold surfaces was performed by the 1-ethyl-3-dimethylaminopropyl carbodiimide (EDC)-mediated coupling reaction between primary amine groups of the chitosan surface and phosphonic acid groups of PolyEGMP grafted on N-HAp. The average weight ($n = 10$) of the chitosan scaffold was 0.02 g. PolyEGMP-grafted N-HAp was dispersed in distilled water (2 mL) at a given weight ratio of chitosan to PolyEGMP-grafted N-HAp (7 : 3 or 3 : 7). The solution was treated in a bath-type ultrasonicator for 30 min, and the uniformly dispersed solution was adjusted to pH 5.8 using a 1 N HCl solution. EDC (a half mole percent of repeating units of PolyEGMP on the N-HAp surfaces) was then added to the solution. The chitosan scaffolds were immersed in the aqueous solution containing uniformly dispersed PolyEGMP-grafted N-HAp and EDC, and the suspension was stirred at room temperature for 48 h. After the reaction, the scaffolds were purified through repeated washing with distilled water. Porous scaffolds with surface-immobilized N-HAp were obtained by freeze-drying for 48 h.

4. Preparation of bulk phase-mixed chitosan/N-HAp scaffolds and chitosan scaffolds

Chitosan (MW: 100 000 g mol^{-1}) powder was dissolved in a 2% (v/v) acetic acid aqueous solution in order to prepare a 3 wt% chitosan solution. The solution was sufficiently mixed with N-HAp under mild stirring for 24 h at room temperature. The weight ratio of chitosan to N-HAp was 76 : 24 or 94 : 6. The solution mixture was placed in a Teflon cylinder mold (diameter = 13 mm, thickness = 12 mm) and frozen at −20 °C for 24 h. The frozen solution was freeze-dried for 48 h to obtain porous chitosan/N-HAp scaffolds. The cylinder-type scaffolds for cell culture were cut into sections 12 mm in diameter with 3 mm thickness. The scaffolds were immersed in a NaOH aqueous solution (1 N) for 24 h to neutralize the remaining acetic acid and were purified by several washings with distilled water. Porous chitosan scaffolds were fabricated using an identical procedure without adding N-HAp.

5. TGA analysis

The amount of immobilized N-HAp on chitosan surfaces was determined by TGA analysis using a SDT Q600 (TA

Instruments, Delaware, USA). The temperature was raised from room temperature to 1000 °C at a rate of 10 °C min^{-1} under a nitrogen atmosphere. The amount of N-HAp was determined as a percentage of the weight loss during heating.

6. Field-emission scanning electron microscopy (FE-SEM)

Morphology observation and surface elemental analyses of porous hybrid scaffolds were performed using a FE-SEM (JSM-6700F, JEOL, Tokyo, Japan). The samples were coated with Pt on a Cressington Scientific Instruments 108 auto sputter coater. The accelerating voltage for SEM images was 15 kV.

7. X-Ray photoelectron spectroscopy (XPS)

XPS experiments were performed on an ESCALAB MK II (V.G. Scientific Co., UK) using monochromatic Al Kα radiation (1486.7 eV) as the excitation source. All spectra were acquired at a pass energy of 80 eV with the anode operated at 300 W. Surface atomic percentages were calculated by normalizing the area of each peak with the total peak area of all atomic elements.

8. Cell culture

Dulbecco's Modified Eagle's medium (DMEM), antibiotic–antimycotic, fetal bovine serum (FBS) and trypsin-EDTA solution were purchased from Gibco (Grand Island, New York, USA). Ascorbic acid, β-glycerol-2-phosphate and dexamethasone were supplemented from Sigma (St. Louis, MO, USA). Human adipose-derived stem cells (ADSCs) were obtained from the Catholic University of Korea. The ADSCs were routinely cultured in 100 cm^2 flasks at 37 °C in a humidified incubator with 5% CO_2. The DMEM medium contained 15% fetal bovine serum and 1% antibiotics (penicillin 100 U mL^{-1}, streptomycin 0.1 mg mL^{-1}), 50 mM ascorbic acid, 0.1 μM dexamethasone and 10 mM β-glycerophosphate. For subculture, the cells were washed twice with phosphate-buffered saline (PBS) and incubated with trypsin-EDTA (ethylene diaminetetraacetic acid) solution (0.05% (w/v) trypsin, 0.02% (w/v) EDTA) for 10 min at 37 °C to detach the cells, and the fresh medium was added at room temperature to inhibit the effect of trypsin. The cells were washed by centrifugation, and resuspended in the medium for reseeding.

9. MTT assay

The extent of cell proliferation on chitosan scaffolds and hybrid scaffolds was measured by a MTT assay, which is based on the mitochondrial conversion of tetrazolium salt, 3-(4,5-dimethylthiazol-2-yl)-2,5-diphenyltetrazolium bromide (MTT). The chitosan and hybrid scaffolds were seeded with NIH3T3 fibroblasts, approximately 5×10^5 cells mL^{-1}, in culture medium and incubated for 1, 3, and 7 days ($n = 3$). Before measurement of MTT assay, chitosan and hybrid scaffolds were washed three times with PBS and were removed. The 20 μL MTT solution (5 mg mL^{-1} MTT in RPMI-1640) and 500 μL DMEM were added to each scaffold and incubated at 37 °C for 4 h in order to allow for formazan formation. After dissolving formazan by adding DMSO (500 μL), the solution of 200 μL was transferred to a 96 well plate. The optical density of each well was read at 570 nm using a microplate reader (Spectra Max 250, Molecular Devices, Sunnyvale, CA).

10. Alkaline phosphatase (ALP) activity

The level of ALP, a marker of osteoblast activity, was measured by the specific conversion of sodium *para*-nitrophenyl-2-phosphate (PNPP) into *para*-nitrophenol (PNP). After 1 week and 5 week cultures, the scaffolds seeded with ADSCs were fixed by a 10% paraformaldehyde solution. The chitosan and hybrid scaffolds were washed with PBS and homogenized with 2 mL lysis buffer solution (0.02% Triton X-100, Sigma) for 2 min. Ground scaffolds were then centrifuged at 14000 rpm for 15 min at 4 °C. Supernatants freshly collected at 1 week and 5 weeks were subjected to assay ($n = 3$). The enzyme reaction was set up by mixing 6 μL of the sample with 54 μL of 0.02% lysis buffer containing 100 μL of 1 M Tris-HCl (Sigma, pH 9.0), 20 μL of 5 mM $MgCl_2$, and 20 μL of 5 mM PNPP. The solution was incubated at 37 °C for 30 min and the reaction was then stopped by 1 N NaOH solution. The level of PNP production was measured by monitoring the light absorbance of the solution at 405 nm using a microplate reader.

11. *In vivo* implantation and estimation of bone tissue formation

ADSCs were seed at 5×10^5 cells mL^{-1} on the chitosan and hybrid scaffolds. Cell-scaffold constructs were maintained in osteogenic differentiation media supplemented with 50 mM ascorbic acid, 0.1 μM dexamethasone, and 10 mM β-glycerophosphate at 37 °C in a humidified incubator with 5% CO_2 for 1 week. Cell-cultured scaffold constructs were implanted into the subcutaneous dorsum of 6 week-old male immunodeficient mice (Jung-Ang Lab Animal Inc., Seoul, Korea) to evaluate their biocompatibility and bone tissue formation. The mice were sacrificed, and the constructs were removed at 4 and 12 weeks after implantation. Retrieved specimens were rinsed with PBS solution and fixed in 10% v/v paraformaldehyde, and embedded in paraffin. The specimens were cut into 5 μm thick sections for staining with hematoxylin and eosin (H&E) for nucleus and cytoplasm, with Masson's trichrome for synthesis of collagen, and with alizarin red S for the biological mineralization of differentiated osteoblasts.

Results and discussion

1. Preparation of surface-repellent stable N-HAp colloids

The surface treatment of N-HAp is useful to immobilize N-HAp at the nano-level on pore surfaces of scaffolds owing to the following two limitations of native N-HAp: since N-HAp itself has limited surface reactivity, it cannot be readily reacted with the polymer surface to form interfacial chemical linkages.[20–22] Furthermore, N-HAp tends to form aggregates and undergo phase separation in solutions due to inter-particle van der Waals interaction/H-bonding as well as its high density (3.2 g mL^{-1}).[23,24] To overcome these limitations of N-HAp, surface modification of N-HAp with PolyEGMP is reasonably effective to provide surface reactivity and colloidal stability, which are two prerequisites for successful surface immobilization on scaffold pore

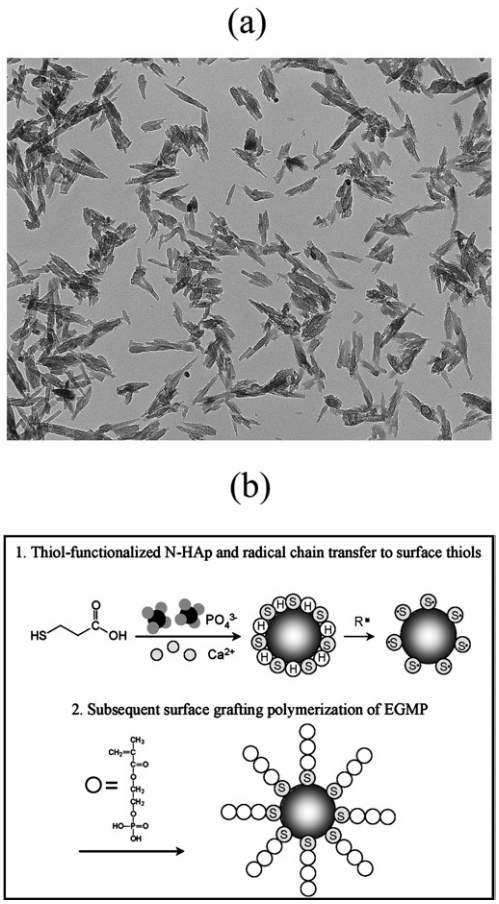

Fig. 1 (a) TEM image of PolyEGMP-grafted N-HAp and (b) illustration of synthesis procedure and detailed mechanism of PolyEGMP grafting on N-HAp surfaces.

surfaces. N-HAp has dimensions of 120 nm in length and 20 nm in width (Fig. 1(a)). The mechanism for PolyEGMP grafting on N-HAp surfaces is briefly illustrated in Fig. 1(b). The radical chain transfer to surface thiol groups generated the sulfur-centered radicals on N-HAp nano-surfaces, which initiated the surface grafting polymerization of EGMP. The ^{1}H NMR spectrum in Fig. 2 identifies the existence of PolyEGMP on N-HAp. PolyEGMP-grafted N-HAp (grafted content of PolyEGMP on N-HAp = 16 wt% (TGA)) showed excellent colloidal stability in

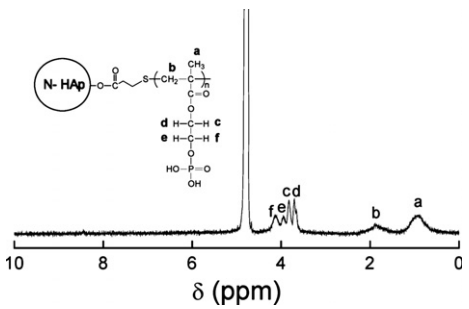

Fig. 2 ^{1}H NMR spectrum of PolyEGMP-grafted N-HAp in D_2O. Resonance peaks a and b are assigned to methyl and methylene protons, respectively, in the PolyEGMP back bone. Peaks c–f are ascribed to ethylene protons neighboring the phosphate group.

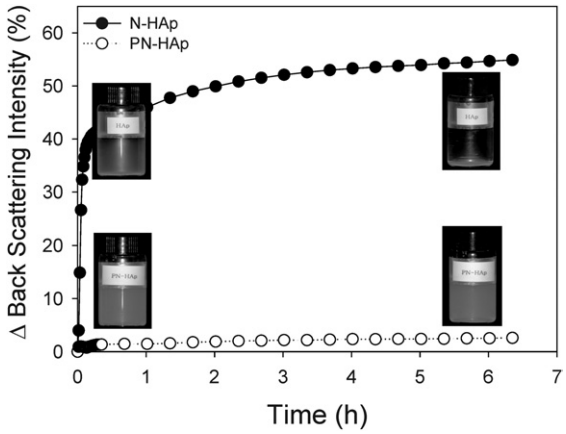

Fig. 3 Kinetic colloidal stability of aqueous N-HAp and PolyEGMP-grafted N-HAp based on time-dependent changes of back scattering intensities (PN-HAp indicates PolyEGMP-grafted N-HAp).

an aqueous phase due to the charge repulsion of surface anionic phosphates ($\zeta = -23$ mV), which was supported by constant back scattering intensity, indicating sedimentation-free solution behavior. As shown in Fig. 3, N-HAp without surface-grafted PolyEGMP does not maintain colloidal stability and precipitates within 5 min. This is reflected by the abrupt increase in Δ(back scattering intensity) due to N-HAp sedimentation. On the other hand, N-HAp with surface-grafted PolyEGMP exhibits excellent colloidal stability and maintains a prolonged stable nano-dispersion state, which is supported by the constant Δ(back scattering intensity).

2. Surface immobilization of N-HAp on pore surfaces of chitosan scaffolds

Scheme 1 illustrates the synthesis approach of porous chitosan scaffolds with surface-immobilized N-HAp. Immobilization of N-HAp was performed by the EDC-mediated coupling reaction between primary amine groups of the chitosan surface and phosphonic acid groups on PolyEGMP-grafted N-HAp. TGA analysis showed that the amount of immobilized N-HAp on the pore surface of chitosan scaffolds could be readily modulated by adjusting the feed amount of PolyEGMP-grafted N-HAp to chitosan (Fig. 4). Chitosan scaffolds with bulk-mixed and surface-immobilized N-HAp were denoted, respectively, as BM-Hybrid and SI-Hybrid, of which the N-HAp contents were identically 6 or 24 wt%. FE-SEM and XPS results in Fig. 5 show surface morphology and element composition of hybrid scaffolds compared to the control chitosan scaffold. It is obvious that surface-modified N-HAp with a needle-like shape is successfully immobilized on the pore surface of chitosan scaffolds, Fig. 5(c), and N-HAp covers the surfaces at the nano-level by forming a N-HAp layer, whereas the surface-exposed N-HAp was not significant in the case of BM-Hybrid. Enlarged surface images in Fig. 6 clearly show that the chitosan surface of SI-Hybrid is decorated with needle-type N-HAp at the nano-level, whereas for BM-Hybrid N-HAp forms micro-scale clusters and exists as a phase-mixed state with chitosan. XPS analyses strongly support the pronounced exposure of N-HAp on the surface of SI-Hybrid.

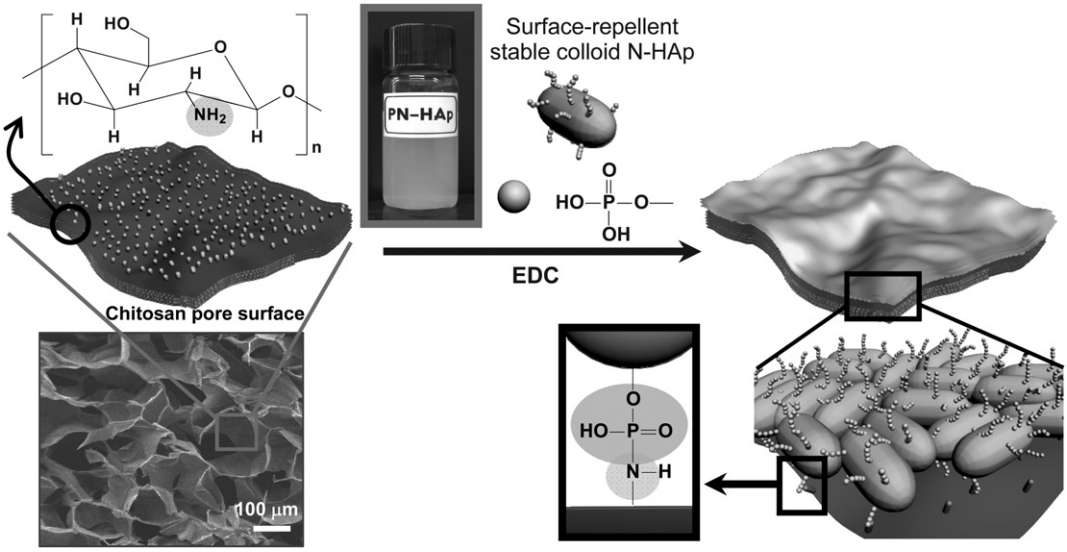

Scheme 1 Schematic illustration for fabrication of porous chitosan scaffolds with surface-immobilized N-HAp (PN-HAp indicates PolyEGMP-grafted N-HAp).

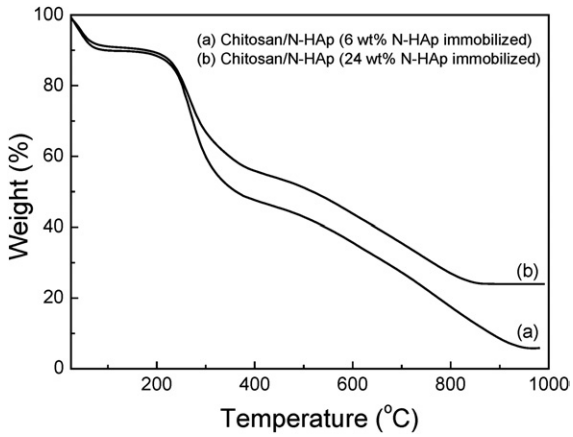

Fig. 4 TGA thermograms of SI-Hybrid scaffolds with the different amount of surface-immobilized N-HAp.

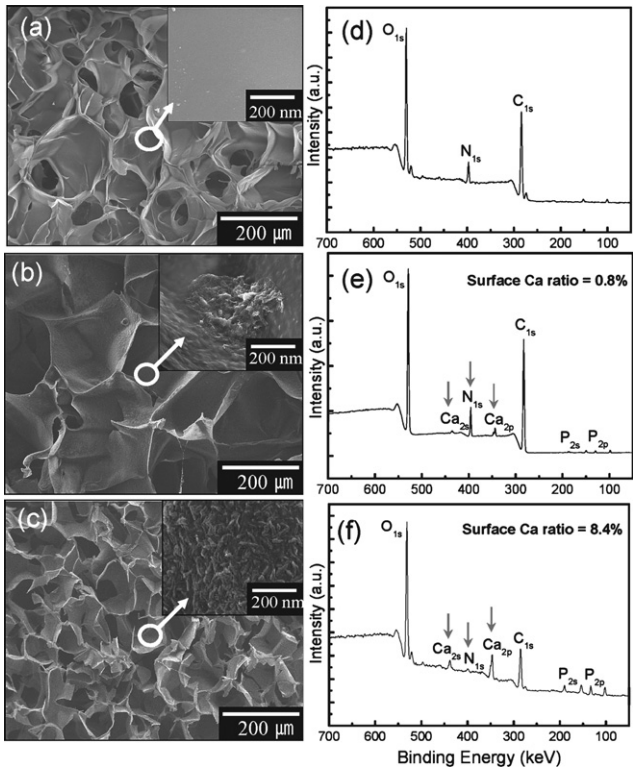

Fig. 5 FE-SEM images and XPS analysis data: (a) and (d) chitosan scaffold, (b) and (e) BM-Hybrid (24 wt% N-HAp bulk-mixed), (c) and (f) SI-Hybrid (24 wt% N-HAp surface-immobilized).

The surface of BM-Hybrid exhibits weak intensity Ca signals (Ca_{2s}, Ca_{2p}) and relatively strong binding energy of nitrogen (N_{1s}) ascribed to chitosan (Fig. 5(e)). This indicates that most phases of N-HAp are embedded within the chitosan bulk phase. On the other hand, for SI-Hybrid in Fig. 5(f), the nitrogen signal of chitosan is negligible, whereas Ca peak intensities are remarkably enhanced, which is not observed with BM-Hybrid. Strikingly, the atomic ratio of Ca on the SI-Hybrid surfaces was found to be 8.4%, which is a 950% increase compared to that on the BM-Hybrid surfaces (0.8%). This indicates that the existence of grafted PolyEGMP on the N-HAp surfaces does not seriously protect exposure of N-HAp phases on chitosan surfaces. XPS analyses also support the successful chemical anchoring of N-HAP on chitosan surfaces. Fig. 7(a) shows that the characteristic P_{2p} peak of PolyEGMP-grafted N-HAp was observed at approximately 133 eV binding energy, which originated from phosphates (PO_4) of N-HAp and surface-grafted PolyEGMP.[25,26] Notably, Fig. 7(b) shows that P_{2p} signals from N-HAp-immobilized scaffolds are split to form the new band, indicating the formation of phosphorus (P) with a new atomic environment. This peak reasonably originated from phosphorus of the P–N linkage, which is formed by the reaction between phosphonic acid of PolyEGMP on N-HAp and primary amines of chitosan surfaces. Thus, it is confirmed that the N-HAp is stably immobilized at the nano-level on the pore surfaces of chitosan scaffolds.

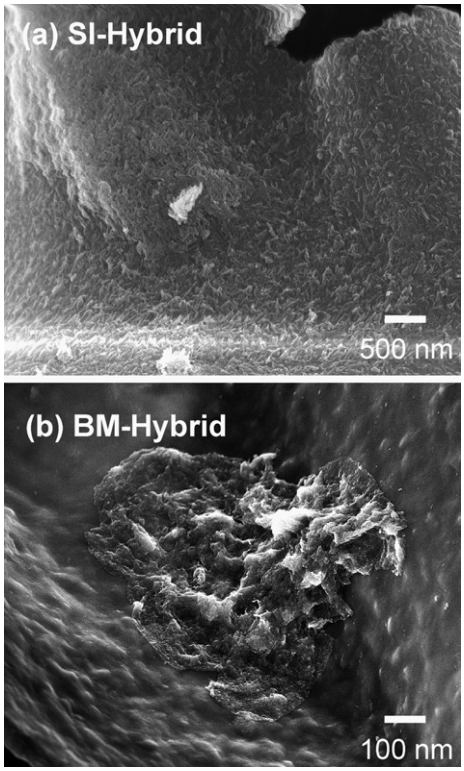

Fig. 6 SEM images of scaffold pore surfaces of (a) SI-Hybrid and (b) BM-Hybrid.

3. *In vitro* evaluation of biocompatibility and osteogenic potential

The effect of N-HAp immobilization on cellular interaction, adhesion, and proliferation was estimated using NIH3T3 fibroblasts. To verify the superiority of scaffolds with surface-immobilized N-HAp in terms of cell growth, various groups of porous scaffolds were fabricated: (I) the chitosan scaffold, (II) the chitosan scaffold with surface-immobilized PolyEGMP, (III) chitosan/N-HAp scaffolds fabricated by a solution bulk mixing (BM-Hybrid), (IV) chitosan scaffolds with surface-immobilized N-HAp (SI-Hybrid). Fig. 8 shows the viability of cells cultured on various porous scaffolds (I–IV). In general, cell growth is somewhat pronounced for scaffolds containing N-HAp over that of the chitosan scaffold, and gradual cell growth was observed with increasing incubation time. Scaffold group II, the chitosan scaffolds with surface-immobilized PolyEGMP, did not show a remarkable effect on cell adhesion and growth. Scaffold group III, fabricated by bulk solution mixing of N-HAp with chitosan, does not provide a surface favorable for effective cell growth, probably because the fabrication process is not effective in exposing N-HAp at the nano-level on the pore surface of scaffolds. It is of great interest to note that the cell adhesion and proliferation on scaffold group IV with surface-immobilized N-HAp are much more remarkable than the control scaffold groups (I–III). After 7 days of culture, the cell viability on scaffold group IV was found to be more than 200% over that of the other hybrid scaffolds III, of which N-HAp surfaces are covered with polymer phases, and thus N-HAp could not be effectively exposed on the scaffold surface. As the content of surface-

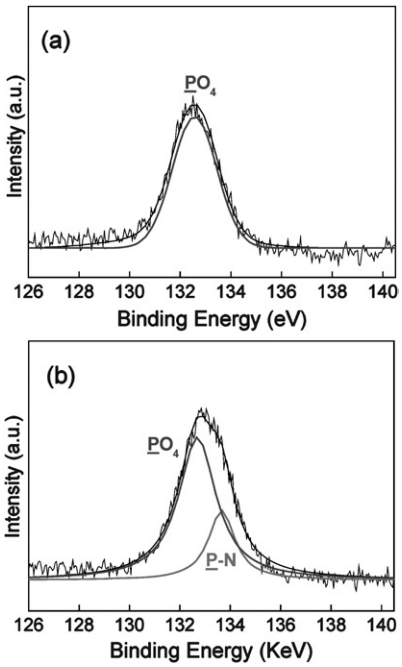

Fig. 7 XPS signals of the P_{2p} region with the associated curve fitting: (a) PolyEGMP-grafted N-HAp and (b) SI-Hybrid (24 wt% N-HAp surface-immobilized).

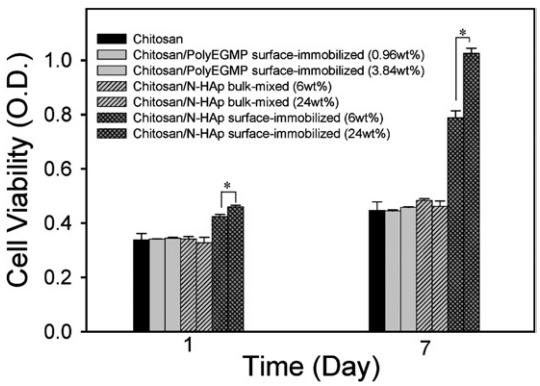

Fig. 8 Viability of NIH3T3 fibroblasts on various classes of porous scaffolds as a function of incubation time ($n = 3$). * $P < 0.01$. Each group is classified based on the fabrication process and presented in an identical bar format.

immobilized N-HAp increased from 6 wt% to 24 wt%, the cell viability was more pronounced. This suggests that surface-located N-HAp is a main contributing factor for effective cell–scaffold interaction as well as cell growth. Since the surfaces of scaffold group IV were covered with PolyEGMP-grafted N-HAp, scaffold group II with surface PolyEGMP, the amount of which was the same as that of grafted-PolyEGMP on N-HAp, was fabricated to give an answer to the question of whether surface-exposed PolyEGMP is a main factor determining the cellular interaction on scaffolds. As described, PolyEGMP itself did not express notable effects on cellular interaction/proliferation in the experimental content range. Conclusively, it is evident that the component which makes the pore surfaces favorable for cellular anchorage and growth is the surface-exposed N-HAp.

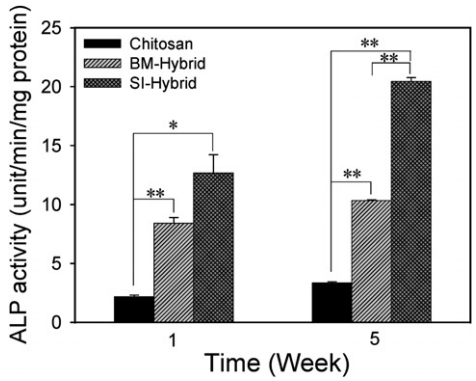

Fig. 9 ALP activity for the chitosan scaffold, BM-Hybrid (24 wt% N-HAp bulk-mixed), and SI-Hybrid (24 wt% N-HAp surface-immobilized) ($n = 3$). * $P < 0.05$, ** $P < 0.01$.

To evaluate the osteoblastic differentiation of human adipose-derived stem cells (ADSCs), we measured the ALP activity of cell–scaffold constructs. As shown in Fig. 9, differentiated ADSCs on hybrid scaffolds showed a significant enhancement in ALP activity during the 5 week culture period, indicating that ADSCs on the hybrid scaffolds exhibited more differentiated osteoblastic behavior than on the control chitosan scaffold. After culture times of 1 week and 5 weeks, the ALP activity of hybrid scaffolds was found to be higher than that of the chitosan scaffold. It is noteworthy that, after five weeks, the ALP activity of SI-Hybrid was found to be significantly higher than that of BM-Hybrid. This indicates that the existence of N-HAp on the pore surface of the chitosan scaffold is stable for a prolonged culture of five weeks and displays a notable effect on the differentiation of ADSCs to osteoblasts

4. *In vivo* implantation and evaluation of bone-tissue formation

In vivo bone-tissue regenerative activity was evaluated by implantation of cell–scaffold constructs in the subcutaneous pouches of immunodeficient mice at 4 and 12 weeks. It was found that scaffold pore structures maintained structural integrity over the implantation time. H&E histological analysis shows that any new tissue formation was not found in cell-free scaffolds, irrespective of the implantation period. The cell-cultured chitosan scaffold in Fig. 10 induces tissue formation, but not to a great extent. The incorporation of N-HAp into chitosan (BM-Hybrid) contributed substantially to the enhanced new tissue formation. It is interesting to note that tissue generation on SI-Hybrid is greatly increased, and the large area of connective woven bone tissues gets thicker with prolonged implantation. Even at the early state of 4 weeks post-implantation, SI-Hybrid already shows enhanced bone tissue formation. After 12 weeks of implantation, the tissue layers are more densely packed. This strongly supports our assumption that surface-immobilized N-HAp on scaffold pores not only provides a favorable environment for bone cell proliferation but also accelerates bone tissue formation in *in vivo* conditions.

During new tissue regeneration, osteoblasts secrete proteins to construct an extracellular matrix (ECM). Collagen, which constitutes approximately 95% of the ECM protein matrix in bones, is a good marker for estimation of bone tissue formation.[9] Collagen formed on the scaffolds was selectively stained as dense blue areas through Masson's trichrome staining. As shown in Fig. 11, at 4 weeks after implantation, SI-Hybrid supports collagen expression more densely than the BM-Hybrid and chitosan scaffolds. Although N-HAp in BM-Hybrid shows substantial effects in terms of collagen formation, its activity was not comparable to N-HAp immobilized on SI-Hybrid. At 12 weeks, it is of interest to note that the connective areas of densely packed blue on SI-Hybrid scaffolds almost cover the entire lumen of scaffolds, as compared with chitosan and BM-Hybrid scaffolds. This indicates that SI-Hybrid promotes new bone formation better than chitosan and BM-Hybrid.

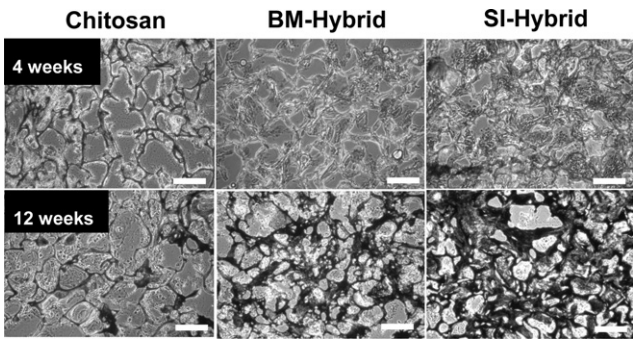

Fig. 11 Masson's trichrome staining of chitosan scaffolds, BM-Hybrid, and SI-Hybrid at 4 and 12 weeks after implantation (scale bars = 200 μm).

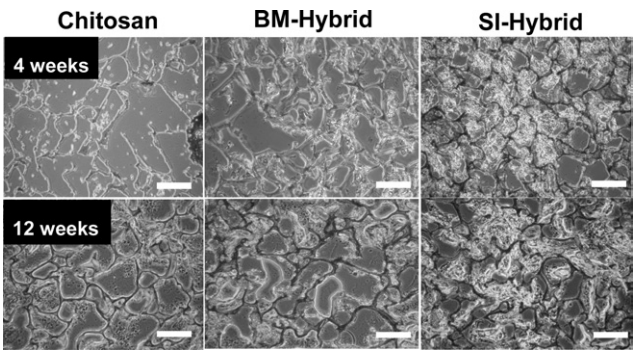

Fig. 10 H&E staining of chitosan scaffolds, BM-Hybrid, and SI-Hybrid at 4 and 12 weeks after implantation (scale bars = 200 μm).

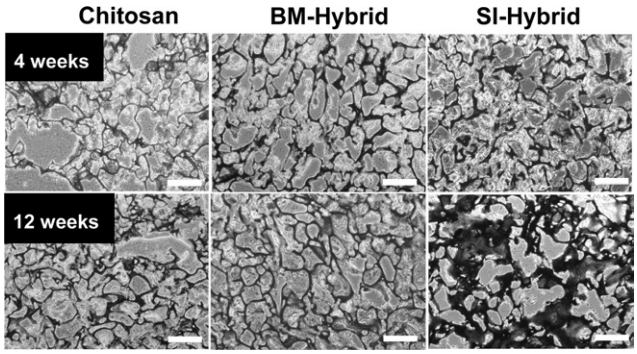

Fig. 12 Alizarin red S staining of chitosan scaffolds, BM-Hybrid, and SI-Hybrid at 4 and 12 weeks after implantation (scale bars = 200 μm).

Fig. 12 shows the stained section images of various classes of scaffolds by alizarin red S after an implantation of 4 and 12 weeks. At 4 and 12 weeks after implantation, calcium deposition is more progressive and extensive for SI-Hybrid. As implantation time increases, the stained area of calcium deposition on SI-Hybrid is found to be much denser, indicating improved osteoconductive properties for bone mineral formation.

Conclusions

We described the rational synthetic approach to novel organic–inorganic hybrid scaffolds for tissue engineering applications. For bone-regenerative porous materials, the benefits of bioactive N-HAp, such as high specific surface areas, excellent protein/cell binding ability and osteoconductivity, can be fully expressed only when it is exposed on the pore surface at the nano-level. The use of self-dispersing reactive N-HAp as a key element could make it possible to immobilize N-HAp discretely on the biocompatible chitosan pore surfaces *via* chemical linkages. The porous chitosan scaffolds with surface-immobilized N-HAp showed much improved surface properties for cell adhesion and growth compared with the conventional polymer/N-HAp scaffolds prepared by simple bulk mixing. In addition, they provided favorable environments for enhanced *in vitro* and *in vivo* osteogenic potential and bone tissue growth, estimated by characteristic biomarkers of bone formation such as ALP and collagen. These results suggest that porous scaffolds with surface-immobilized N-HAp can serve as improved alternatives to current hybrid scaffolds for bone tissue engineering. Since the surfaces of a broad range of biomaterials including polymers, ceramics and metals can be functionalized with amine groups, N-HAp can be readily anchored on surfaces to generate many classes of bone-compatible, bioactive scaffolds, irrespective of scaffold type, such as fibrous scaffolds or porous microsphere-type scaffolds. In addition, the presence of functional phosphonic acid groups on the immobilized N-HAp surface can provide an opportunity for further functionalization with specific cell-binding ligands or growth factors. The nano-scale engineering described in this work may have general significance in the generation of bioactive cell-compatible/tissue-regenerative surfaces of many classes of biomaterials with any shape and dimensions.

Acknowledgements

This research was supported by a grant (code #: 08K1501-01110) from 'Center for Nanostructured Materials Technology' under '21st Century Frontier R&D Programs' of the Ministry of Education, Science and Technology, Korea. The authors thank Dr Se Geun Lee and Sung Jun Lee of DGIST for their technical assistance.

References

1 G. Wei and P. X. Ma, *Biomaterials*, 2004, **25**, 4749.
2 S.-S. Kim, M. S. Park, O. Jeon, C. Y. Choi and B.-S. Kim, *Biomaterials*, 2006, **27**, 1399.
3 T. Kaneko, D. Ogomi, R. Mitsugi, T. Serizawa and M. Akashi, *Chem. Mater.*, 2004, **16**, 5596.
4 Z. Hong, P. Zhang, C. He, X. Qiu, A. Liu, L. Chen, X. Chen and X. Jing, *Biomaterials*, 2005, **26**, 6296.
5 J. D. Hartgerink, E. Beniash and S. I. Stupp, *Science*, 2001, **294**, 1684.
6 W. Traub, T. Arad and S. Weiner, *Proc. Natl. Acad. Sci. U. S. A.*, 1989, **86**, 9822.
7 E. N. Antonov, V. N. Bagratashvili, M. J. Whitaker, J. J. A. Barry, K. M. Shakesheff, A. N. Konovalov, V. K. Popov and S. M. Howdle, *Adv. Mater.*, 2005, **17**, 327.
8 C. J. Bettinger, E. J. Weinberg, K. M. Kulig, J. P. Vacanti, Y. Wang, J. T. Borenstein and R. Langer, *Adv. Mater.*, 2006, **18**, 165.
9 W. Sun, J. E. Puzas, T.-J. Sheu, X. Liu and P. M. Fauchet, *Adv. Mater.*, 2007, **19**, 921.
10 C. R. Kothapalli, M. T. Shaw and M. Wei, *Acta Biomater.*, 2005, **1**, 653.
11 H. J. Chung and T. G. Park, *Adv. Drug Delivery Rev.*, 2007, **59**, 249.
12 W. L. Murphy and D. J. Mooney, *J. Am. Chem. Soc.*, 2002, **124**, 1910.
13 J. Song, E. Saiz and C. R. Bertozzi, *J. Am. Chem. Soc.*, 2003, **125**, 1236.
14 J. Song, V. Malathong and C. R. Bertozzi, *J. Am. Chem. Soc.*, 2005, **127**, 3366.
15 T. Kokubo, *Acta Mater.*, 1998, **46**, 2519.
16 W. J. Landis, F. H. Silver and J. W. Freeman, *J. Mater. Chem.*, 2006, **16**, 1495.
17 T. J. Webster, C. Ergun, R. H. Doremus, R. W. Siegel and R. Bizios, *J. Biomed. Mater. Res.*, 2000, **51**, 475.
18 H. J. Lee, S. E. Kim, H. W. Choi, C. W. Kim, K. J. Kim and S. C. Lee, *Eur. Polym. J.*, 2007, **43**, 1602.
19 S. C. Lee, H. W. Choi, H. J. Lee, K. J. Kim, J. H. Chang, S. Y. Kim, J. Choi, K.-S. Oh and Y.-K. Jeong, *J. Mater. Chem.*, 2007, **17**, 174.
20 X. Qiu, Z. Hong, J. Hu, L. Chen, X. Chen and X. Jing, *Biomacromolecules*, 2005, **6**, 1193.
21 H. J. Lee, H. W. Choi, K. J. Kim and S. C. Lee, *Chem. Mater.*, 2006, **18**, 5111.
22 Q. Liu, J. R. de Wijn and C. A. van Blitterswijk, *J. Biomed. Mater. Res.*, 1998, **40**, 257.
23 G. Ciapetti, L. Ambrosio, L. Savarino, D. Granchi, E. Cenni, N. Baldini, S. Pagani, S. Guizzardi, F. Causa and A. Giunti, *Biomaterials*, 2003, **24**, 3815.
24 H. W. Choi, H. J. Lee, K. J. Kim, H.-M. Kim and S. C. Lee, *J. Colloid Interface Sci.*, 2006, **304**, 277.
25 C. C. Chusuei, D. W. Goodman, M. J. van Stipdonk, D. R. Justes and E. A. Schweikert, *Anal. Chem.*, 1999, **71**, 149.
26 I. Minami, K. Hirao, M. Memita and S. Mori, *Tribol. Int.*, 2007, **40**, 626.